Hybrid density functional study of small Rh$_n$ ($n = 2-15$) clusters

Juarez L. F. Da Silva,[1,2,*] Maurício J. Piotrowski,[2,†] and F. Aguilera-Granja[3,‡]

[1]*Instituto de Química de São Carlos, Universidade de São Paulo, Caixa Postal 780, 13560-970 São Carlos, São Paulo, Brazil*
[2]*Instituto de Física de São Carlos, Universidade de São Paulo, Caixa Postal 369, 13560-970 São Carlos, São Paulo, Brazil*
[3]*Instituto de Física, Universidad Autónoma de San Luis Potosí, 78000 San Luis Potosí, Mexico*

The physical properties of small rhodium clusters, Rh$_n$, have been in debate due to the shortcomings of density functional theory (DFT). To help in the solution of those problems, we obtained a set of putative lowest energy structures for small Rh$_n$ ($n = 2$–15) clusters employing hybrid-DFT and the generalized gradient approximation (GGA). For $n = 2$–6, both hybrid and GGA functionals yield similar ground-state structures (compact), however, hybrid favors compact structures for $n = 7$–15, while GGA favors open structures based on simple cubic motifs. Thus, experimental results are crucial to indicate the correct ground-state structures, however, we found that a unique set of structures (compact or open) is unable to explain all available experimental data. For example, the GGA structures (open) yield total magnetic moments in excellent agreement with experimental data, while hybrid structures (compact) have larger magnetic moments compared with experiments due to the increased localization of the 4d states. Thus, we would conclude that GGA provides a better description of the Rh$_n$ clusters, however, a recent experimental-theoretical study [Harding *et al.*, J. Chem. Phys. **133**, 214304 (2010)] found that only compact structures are able to explain experimental vibrational data, while open structures cannot. Therefore, it indicates that the study of Rh$_n$ clusters is a challenging problem and further experimental studies are required to help in the solution of this conundrum, as well as a better description of the exchange and correlation effects on the Rh$_n$ clusters using theoretical methods such as the quantum Monte Carlo method.

I. INTRODUCTION

Transition-metal (TM) particles with a few (clusters) to a hundred atoms have been widely studied to obtain a better atomistic understanding for a large number of phenomena,[1,2] namely, mechanisms that drive the size evolution from clusters to microscopic particles,[1–3] the size dependence of the catalytic activity of TM nanoparticles (NPs),[1,2,4,5] and the encapsulation of TM particles inside carbon cages (fullerenes or nanotubes).[6–8] Among the 3d, 4d, and 5d TM clusters, rhodium clusters (Rh$_n$) have attracted great interest due to the wide range of applications in catalysis.[6,9] Furthermore, experimental studies reported unexpected large magnetic moments for Rh$_n$ ($n = 9$–34),[10] which is in contrast with the nonmagnetic crystalline phase of bulk Rh.[11] Beyond that, density functional theory (DFT) calculations within local and semilocal functionals have reported low coordinated structures for the lowest energy Rh$_n$ configurations ($6 \leqslant n \leqslant 20$),[12–17] which are based on cubic unit motifs and in contrast with the compact face-centered cubic (fcc) structure of the ground-state crystalline Rh phase.[11]

In order to improve the atomistic understanding of those problems, a wide range of experimental and theoretical studies have been reported for rhodium clusters in the neutral, cationic, and anionic states. Most of the studies have addressed the atomic structure of Rh$_n$ as a function of size,[12–27] the vibrational spectra,[24,25,28] magnetic moments,[3,10,12,14,16,18,22] polarizabilities,[16,29] and the catalytic activity for small molecules.[21,30–34]

Among those studies, hybrid-DFT calculations combined with experimental far-infrared multiple photon dissociation[24,25] have reported that Rh$_n^+$ clusters have compact structures based on octahedron motifs for $n = 6$–12 (i.e.,

only compact structures can explain the vibrational spectra). This finding is consistent with recent screened hybrid-DFT calculations reported for Rh$_{13}$,[27] which identified that an increase in the amount of exact Fock exchange in the hybrid functionals favors compact structures for Rh$_{13}$, and hence, in better agreement with vibrational data.[24,25]

However, it has been reported that low coordinated Rh$_n$ structures obtained by plain DFT calculations yield magnetic moments m_T, in good agreement with experimental results.[10,12–16] For example, plain DFT yields $m_T = 0.69$ μ_B/atom for Rh$_{13}$, while results have obtained 0.48 ± 0.13 μ_B/atom,[10] however, hybrid-DFT calculations yield higher magnetic moments for compact Rh$_n$ clusters (i.e., $m_T = 1.62$ μ_B/atom for Rh$_{13}$).[27] Therefore, the deviation between theory and experimental is substantially larger for hybrid-DFT calculations.

Thus, hybrid-DFT calculations yield compact structures and vibrational spectra in better agreement with experimental results,[24,25] however, the magnetic moments are too high compared with the experimental results.[10,27] In contrast, plain DFT yields open structures, which does not explain the vibrational spectra,[24,25] however, it yields total magnetic moments in excellent agreement with experimental results.[10]

Therefore, several questions remain open, and a better understanding of the evolution of the Rh$_n$ clusters as a function of size using hybrid-DFT calculations is required. In this work, we will investigate the lowest energy structures of the Rh$_n$ clusters ($n = 2$–15) employing screened hybrid-DFT and plain DFT calculations, and hence, the value of n for which the hybrid-DFT and plain DFT framework yield different lowest energy Rh$_n$ structures can be identified.
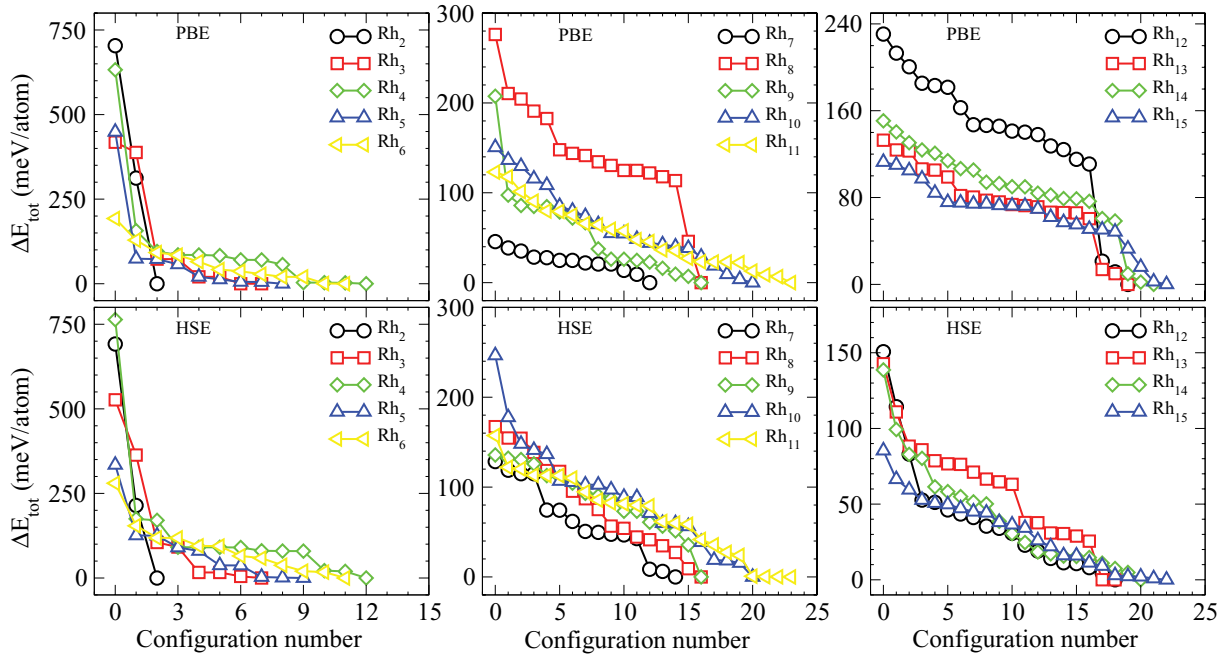
FIG. 1. (Color online) Relative total energies ΔE_{tot} for the Rh_n clusters calculated with the PBE and HSE functionals. $\Delta E_{\text{tot}} = E_{\text{tot}}^{Rh_n^i} - E_{\text{tot}}^{Rh_n^{\text{lowest}}}$.

II. THEORETICAL APPROACH AND COMPUTATIONAL DETAILS

Our calculations are based on spin-polarized DFT calculations within two approximations for the exchange-correlation (xc) energy functional: (i) The generalized gradient approximation (GGA) formulated by Perdew, Burke, and Ernzerhof (PBE).[35] (ii) The screened Coulomb hybrid xc functional proposed by Heyd, Scuseria, and Ernzerhof (HSE),[36,37] which was derived from the hybrid PBE0 functional.[38,39] In hybrid functionals such as PBE0, a fraction of the exchange part of PBE, E_x^{PBE}, is replaced by the nonlocal Fock exchange, E_x^{HF},[38] while the correlation part is taken as the one in the standard PBE formulation, E_c^{PBE}.[35] Thus, $E_{xc}^{\text{hybrid}} = (1 - \alpha_{\text{HF}})E_x^{\text{PBE}} + \alpha_{\text{HF}}E_x^{\text{HF}} + E_c^{\text{PBE}}$. The screened hybrid HSE functional is obtained using a complementary error function to cut off the long-range tail of the Coulomb $1/r$ kernel in the E_x^{HF},[36,37] and a screening parameter of 0.109 Å has been suggested based on the calculations for a large number of systems.[40]

The adiabatic-connection fluctuation dissipation theorem[38] suggests a value of 0.25 for α_{HF}, however, several first-principles calculations have suggested that the value of 0.25 for α_{HF} is not capable of yielding results in good agreement with experimental results for all systems and problems.[27,41] In this work, we used a value of 0.15 for α_{HF}, which was obtained in previous work[27] and yields excellent results for Rh_2, Rh_{13}, and bulk Rh. We would like to point out that 25% of exact Fock exchange cannot provide a correct description for bulk Rh,[27] that is, it yields the hexagonal close-packed (hcp) structure as the ground-state bulk structure instead of the observed fcc structure.[11]

The Kohn-Sham equations are solved using the projector augmented wave (PAW) method,[42,43] as implemented in VASP.[44,45] The interaction between the ionic cores and valence electrons is described by the PAW projectors provided within VASP. A cutoff energy of 272 eV was used for all Rh_n ($n = 2$–15) calculations with a single k point (Γ) for the Brillouin-zone integration. The cluster calculations were performed using a cubic box of 14 Å, which yields a large distance between the images. The total energy convergence was set to 10^{-6} and Rh_n structures were optimized until the atomic forces were smaller than 0.025 eV/Å.

A large number of atomic configurations were calculated for Rh_n ($n = 2$–15): (i) Compact structures based on the close-packed units and on Lennard-Jones clusters obtained with the Basin-Hopping Monte Carlo algorithm.[46] (ii) Open structures based on the cubic motifs. (iii) Structures designed by adding a single Rh atom on the lowest energy Rh_{n-1} structures. (iv) Atomic structures reported in the literature.[3,12–16,18,23–26,47] (v) A large number of different magnetic configurations were calculated for every atomic structure.

The analysis of the coordination and bond lengths for all Rh_n clusters were performed using the effective coordination concept,[48–50] which yields the weighted bond lengths d_{av}^i, and effective coordination number ECN_i, for any cluster geometry, where the index i indicates the atom number. In this work, ECN and d_{av} indicate the average overall values assumed by ECN_i and d_{av}^i for a given Rh_n cluster. This approach has been employed in several studies of, for example, bulk oxides and TM clusters.[17,50–52]

III. RESULTS

a. Relative total energies. Following the procedure outlined in Sec. II, we calculated a large number of cluster configurations, which were organized according to the relative

total energies,

$$\Delta E_{\text{tot}} = E_{\text{tot}}^{\text{Rh}_n^i} - E_{\text{tot}}^{\text{Rh}_n^{\text{lowest}}}, \qquad (1)$$

where $E_{\text{tot}}^{\text{Rh}_n^i}$ and $E_{\text{tot}}^{\text{Rh}_n^{\text{lowest}}}$ are the total energies of a given Rh_n^i configuration and of the lowest energy $\text{Rh}_n^{\text{lowest}}$ configuration, respectively. The ΔE_{tot} results are shown in Fig. 1, where it can be seen that the total energies of the calculated Rh_n structures are spread over a wide range of energies, which indicates that a wide range of local environments and different spin configurations were calculated. For particular Rh_n clusters, we noticed a few different configurations with similar energy near the lowest energy structure, which we will discuss below.

b. Lowest energy configurations. The putative lowest energy structures are shown in Fig. 2. For a few systems, we found isomers with close total energies but with different ECN and/or different magnetic moments, and hence, those structures are also shown in Fig. 2. Using the criterion $\Delta E_{\text{tot}} < 10$ meV/atom, the number of isomers is not the same for all Rh_n clusters, for example, for PBE, there are two isomers for $n = 4,5,7,13,15$, and three for $n = 9,10,11,14$, which have differences in the total magnetic moment, except for Rh_5 (differences in the ECN values). For HSE, there are two isomers for $n = 5,8$, three for $n = 7,12,14$, and six for $n = 15$, which differ on the total magnetic moment and coordination environment. Thus, at real experimental conditions, we would expect that a wide range of magnetic moments and slightly different structures might be present. Therefore, to obtain the most important properties, such as the binding energy, total magnetic moments, ECN, and d_{av}, we average the results for the clusters with almost the same energy, that is, $\Delta E_{\text{tot}} < 5.0$ meV/atom, which are shown in Fig. 3, and will be discussed in the next sections.

Our lowest energy hybrid-DFT configurations and the Rh_n structures that yield the best agreement with experimental spectra[25] are in good agreement. For $n = 6$–9, 11, the shape of the structures are in excellent agreement, which indicates that hybrid-DFT calculations using a different percentage of the exact Fock exchanges (25% in Ref. 25 and 15% in this work) yield almost the same structures. However, the same level of agreement is not obtained for $n = 10$ and 12, for which our configurations have lower energies and are slightly more compact than those lowest energy structures reported in Ref. 25. For example, our lowest energy Rh_{10} and Rh_{12} structures are 0.81 and 0.18 eV, respectively, lower than the reported structures in the neutral state.[25]

c. Effective coordination number. The results for ECN are shown in Figs. 2 and 3. For $n = 2$–6, the ECN results using both PBE and HSE functionals are very similar. PBE yields two degenerated isomers for Rh_4, that is, the lowest energy tetrahedron (T_d, ECN = 3.00) structure and a distorted tetrahedron (ECN = 2.55) with higher energy ($\Delta E_{\text{tot}} = 3$ meV/atom), while HSE yields a slightly distorted tetrahedron configuration (ECN = 2.86). For $n = 5$, both PBE (ECN = 3.08, 3.18) and HSE (ECN = 3.06, 3.12) functionals yield structures with lower coordination than an ideal high-symmetry Lennard-Jones (LJ) cluster (ECN = 3.60). For $n = 6$, both functionals yield the same high-symmetry structure (O_h, ECN = 4.0),

which has the same symmetry and coordination of a compact LJ_6 cluster.

For $n = 7$–15, there are clear differences between the PBE and HSE results, that is, the HSE structures are substantially more compact than the PBE lowest energy configurations, however, we would like to point out that the HSE structures have lower ECN than the LJ clusters; see Fig. 3. From test calculations, the differences between ECN for HSE and LJ clusters decrease by increasing the amount of exact exchange in the HSE functional, however, we would like to mention that 25% favors the hcp structure for bulk Rh instead of the experimentally observed fcc structure.[11]

The PBE structures are based on the cubic unit motif (i.e., Rh_8 forms an almost perfect cubic unit), which has been reported in previous studies.[12,14,53] Rh_{12} forms two cubic units, and the intermediate structures are based on those motifs. The HSE structures are very likely the LJ clusters, however, with large distortions, which explains the smaller values for ECN. Hybrid functionals have been known to favor single occupation of the electronic states, and hence, HSE often breaks the symmetry of those clusters by opening a split between degenerate states partially occupied, which lower the energy of the Rh_n clusters.

d. Average weighted bond lengths. The results for d_{av} are shown in Figs. 2 and 3. The bond lengths are about the same for both PBE and HSE functionals for $n = 2$–6 (i.e., PBE and HSE yield similar bond lengths once the structure is about the same), which is expected as both PBE and HSE yield similar equilibrium lattice constants for Rh bulk in the fcc structure. However, there is a clear difference in the weighted bond lengths for $n = 7$–15 (i.e., $d_{\text{av}}^{\text{PBE}} < d_{\text{av}}^{\text{HSE}}$ by about 5.8% for $n = 13$), which can be explained by differences in the coordination environment of the Rh_n clusters. For example, open structures based on the cubic units have smaller values for d_{av} due to the smaller coordination environment that implies that a larger number of electrons are shared by a small number of bonds, and hence, it results in stronger and shorter bond lengths.

e. Binding energy. In order to improve our analysis, we calculate the binding energy per atom, E_b, of the Rh_n clusters with respect to the free atoms,

$$E_b = E_{\text{tot}}^{\text{lowest energy}} - E_{\text{tot}}^{\text{free atom}}, \qquad (2)$$

where $E_{\text{tot}}^{\text{lowest energy}}$ and $E_{\text{tot}}^{\text{free atom}}$ are the total energies per atom of the lowest energy clusters ($\Delta E_{\text{tot}} < 5$ meV/atom) and free atoms, respectively. It can be seen in Fig. 3 that E_b follows the same trend for both PBE and HSE functionals (i.e., the binding energy per atom increases and tends to reach a particular value at the limit of large n). The energy difference between the PBE and HSE is not constant as a function of n (e.g., it is 0.58 eV for Rh_2 and 0.81 eV for Rh_{15}), which indicates that large particles are more affected by an increase in the localization of the d states than small molecules.

For Rh_2, for which there is available experimental binding energy data,[54,55] we obtained -1.70 eV (PBE) and -1.13 eV (HSE), while the experimental results are -1.42 ± 0.13 eV[54] and -1.20 ± 0.00025 eV.[55] Thus, PBE overbinding, which is not very common for DFT-PBE, and HSE slightly underbinding the Rh_2 molecule, however, we would like to mention
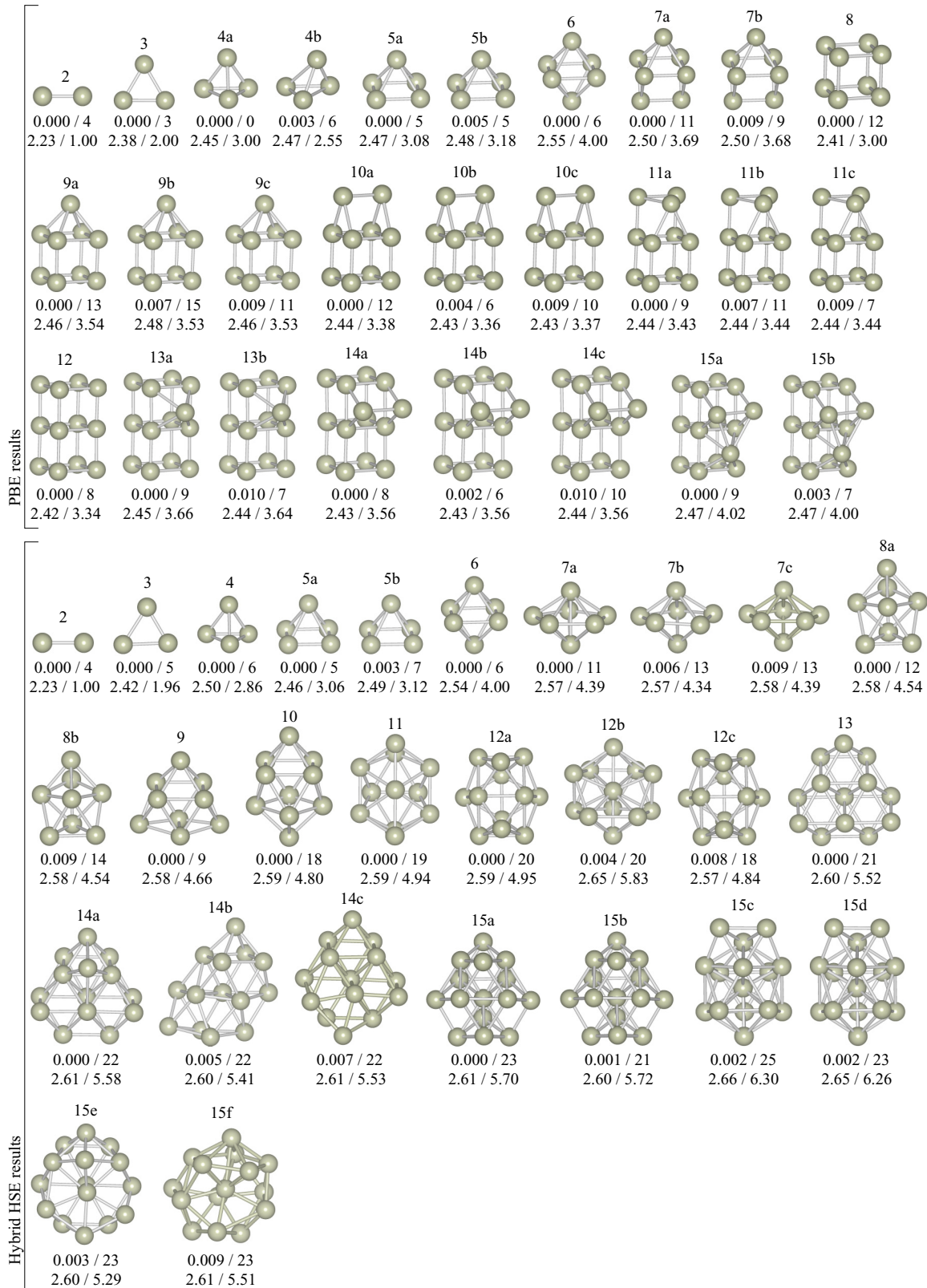
FIG. 2. (Color online) Lowest energy atomic structures for the Rh$_n$ ($n = 2$–15) clusters calculated with the PBE and HSE functionals. High-energy configurations (i.e., $\Delta E_{tot} < 10$ meV/atom) are also reported. Below every cluster, we provided the relative total energy, ΔE_{tot} (eV/atom), and total magnetic moment m_T (μ_B) in the first line, and the average weighted bond lengths d_{av} (Å) and the average effective coordination number ECN in the second line.
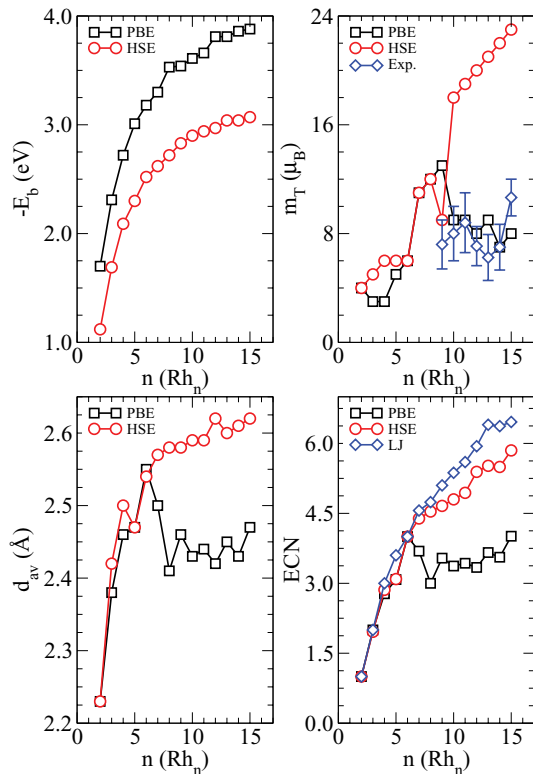
FIG. 3. (Color online) Binding energy per atom E_b, total magnetic moment m_T, average weighted bond lengths d_{av}, and effective coordination number ECN of the Rh$_n$ ($n = 2$–15) clusters calculated with the PBE and HSE functionals. For the Rh$_n$ systems with several degenerated configurations ($\Delta E_{tot} < 5$ meV/atom) an average of the properties were performed. The experimental magnetic data are from Ref. 10.

that the difference between the available experimental results is about 0.2 eV (i.e., quite substantial compared with the differences involved).

f. Total magnetic moments. The total magnetic moments m_T, calculated with PBE and HSE, are shown in Fig. 3 along with the experimental results for $n = 9$–15 within the error bars.[10] We found that $m_T^{PBE} = m_T^{HSE}$ for $n = 2, 6, 7, 8$, $m_T^{PBE} > m_T^{HSE}$ for $n = 9$, and $m_T^{PBE} \leqslant m_T^{HSE}$ for the remaining systems. In particular for $n \geqslant 10$, the differences between PBE and HSE results increase substantially, for example, for Rh$_{13}$, $m_T = 9 \mu_B$ (PBE) and 21 μ_B (HSE). This large difference can be attributed to the following effects: (i) HSE yields a spurious total magnetic moment per atom for the face-centered bulk

Rh of ~0.15 μ_B/atom, while PBE yields zero μ_B, which is consistent with experimental observations for the bulk phase. (ii) For $n \geqslant 10$, the HSE structures are more compact and have higher symmetry, which contributes to narrowing the d states, and hence, contributes to enhancing the total magnetic moment. (iii) The HSE functional yields an increase in the localization of the $4d$ states, which affects the total magnetic moment as well. Therefore, due to the large difference between both PBE and HSE functionals, it is unlikely that both calculations can be explained by the experimental results,[10] which is in fact the case. The PBE results are clearly in better agreement with the experimental results than those obtained by HSE, which favors large magnetic moments.

IV. SUMMARY

In this work, we performed PBE and HSE (15% of exact exchange) calculations for the Rh$_n$ ($n = 2$–15) clusters. We found that both functionals yield similar lowest energy structures for $n = 2$–6, however, both PBE and HSE yield very different lowest energy structures for $n = 7, \ldots, 15$ (i.e., HSE favors compact structures with ECN quite close to the well-known compact LJ clusters), while PBE favors open structures based on cubic motifs. Our lowest energy HSE structures are consistent with the results reported in Ref. 25 for $n = 6$–9, 11, however, for $n = 10$ and 12, we identified lowest energy compact structures. Thus, our HSE structures can yield similar vibrational spectra as those reported in Ref. 25, however, as pointed out in this work, compact Rh$_n$ structures yield very large total magnetic moments, which are far from the experimental values. The low coordinated PBE structures yield magnetic moments in excellent agreement with experimental results, however, open structures are unable to explain the vibrational spectra as pointed out in Ref. 25. Thus, our study indicates that further experimental investigations are required to improve the understanding of the magnetic properties and vibrational spectra of Rh$_n$ clusters, and/or the use of methods such as quantum Monte Carlo, which can provide a correct description of the exchange and correlation effects on equal footing.

*Corresponding author: juarez_dasilva@iqsc.usp.br

†mauriciomjp@gmail.com

‡faustino@dec1.ifisica.uaslp.mx

[1]J. A. Alonso, Chem. Rev. **100**, 637 (2000).

[2]F. Baletto and R. Ferrando, Rev. Mod. Phys. **77**, 371 (2005).

[3]F. Aguilera-Granja, J. M. Montejano-Carrizalez, and R. A. Guirado-López, Phys. Rev. B **73**, 115422 (2006).

[4]Z. Xu, F.-S. Xiao, S. K. Purnell, O. Alexeev, S. Kawi, S. E. Deutsch, and B. C. Gates, Nature (London) **372**, 346 (1994).

[5]S. Vajda, M. J. Pellin, J. P. Greeley, C. L. Marshall, L. A. Curtiss, G. A. Ballentine, J. W. Elam, S. Catillon-Mucherie, P. C. Redfern, F. Mehmood *et al.*, Nat. Mater. **8**, 213 (2009).

[6]X. Pan, Z. Fan, W. Chen, Y. Ding, H. Luo, and X. Bao, Nat. Mater. **6**, 507 (2007).

[7]C. Soldano, F. Rossella, V. Bellani, S. Giudicatti, and S. Kar, ACS Nano **4**, 6573 (2010).

[8]P. Tereshchuk and J. L. F. Da Silva, Phys. Rev. B **85**, 195461 (2012).

[9]B. E. Nieuwenhuys, Adv. Catal. **44**, 259 (2000).

[10]A. J. Cox, J. G. Louderback, S. E. Apsel, and L. A. Bloomfield, Phys. Rev. B **49**, 12295 (1994).

[11]C. Kittel, *Introduction to Solid State Physics*, 7th ed. (John Wiley & Sons, New York, 1996).

[12]Y.-C. Bae, H. Osanai, V. Kumar, and Y. Kawazoe, Phys. Rev. B **70**, 195413 (2004).

[13]W. Zhang, H. Zhao, and L. Wang, J. Phys. Chem. B **108**, 2140 (2004).

[14]Y.-C. Bae, V. Kumar, H. Osanai, and Y. Kawazoe, Phys. Rev. B **72**, 125427 (2005).

[15]S. Li, H. Li, J. Liu, X. Xue, Y. Tian, H. He, and Y. Jia, Phys. Rev. B **76**, 045410 (2007).

[16]F. Aguilera-Granja, L. C. Balbás, and A. Vega, J. Phys. Chem. A **113**, 13483 (2009).

[17]M. J. Piotrowski, P. Piquini, and J. L. F. Da Silva, Phys. Rev. B **81**, 155446 (2010).

[18]F. Aguilera-Granja, J. L. Rodríguez-López, K. Michaelian, E. O. Berlanga-Ramírez, and A. Vega, Phys. Rev. B **66**, 224410 (2002).

[19]L. Wang and Q. Ge, Chem. Phys. Lett. **366**, 368 (2002).

[20]T. Futschek, M. Marsman, and J. Hafner, J. Phys.: Condens. Matter **17**, 5927 (2005).

[21]D. Harding, S. R. Mackenzie, and T. R. Walsh, J. Phys. Chem. B **110**, 18272 (2006).

[22]F. Aguilera-Granja, A. García-Fuente, and A. Vega, Phys. Rev. B **78**, 134425 (2008).

[23]V. Bertin, R. Lopez-Rendón, G. Del Angel, E. Poulain, R. Avilés, and V. UC-Rosas, Int. J. Quantum Chem. **110**, 1152 (2010).

[24]D. J. Harding, T. R. Walsh, S. M. Hamilton, W. S. Hopkins, S. R. Mackenzie, P. Gruene, M. Haertelt, G. Meijer, and A. Fielicke, J. Chem. Phys. **132**, 011101 (2010).

[25]D. J. Harding, P. Gruene, M. Haertelt, G. Meijer, A. Fielicke, S. M. Hamilton, W. S. Hopkins, S. R. Mackenzie, S. P. Neville, and T. R. Walsh, J. Chem. Phys. **133**, 214304 (2010).

[26]M. A. Mora, M. A. Mora-Ramírez, and M. F. Rubio-Arroyo, Int. J. Quantum Chem. **110**, 2541 (2010).

[27]M. J. Piotrowski, P. Piquini, L. Cândido, and J. L. F. Da Silva, Phys. Chem. Chem. Phys. **13**, 17242 (2011).

[28]H. Wang, H. Haouari, R. Craig, Y. Liu, J. R. Lombardi, and D. M. Lindsay, J. Chem. Phys. **106**, 2101 (1997).

[29]M. K. Beyer and M. B. Knickelbein, J. Chem. Phys. **126**, 104301 (2007).

[30]I. Balteanu, O. P. Balaj, B. S. Fox-Beyer, P. Rodrigues, M. T. Barros, A. M. C. Moutinho, M. L. Costa, M. K. Beyer, and V. E. Bondybey, Organometallics **23**, 1978 (2004).

[31]C. Adlhart and E. Uggerud, J. Chem. Phys. **123**, 214709 (2005).

[32]M. S. Ford, M. L. Anderson, M. P. Barrow, D. P. Woodruff, T. Drewello, P. J. Derricka, and S. R. Mackenzie, Phys. Chem. Chem. Phys. **7**, 975 (2005).

[33]C. Adlhart and E. Uggerud, Int. J. Mass Spectrom. **249–250**, 191 (2006).

[34]M. L. Anderson, M. S. Ford, P. J. Derrick, T. Drewello, D. P. Woodruff, and S. R. Mackenzie, J. Phys. Chem. A **110**, 10992 (2006).

[35]J. P. Perdew, K. Burke, and M. Ernzerhof, Phys. Rev. Lett. **77**, 3865 (1996).

[36]J. Heyd, G. E. Scuseria, and M. Ernzerhof, J. Chem. Phys. **118**, 8207 (2003).

[37]J. Heyd and G. E. Scuseria, J. Chem. Phys. **120**, 7274 (2004).

[38]J. P. Perdew, M. Ernzerhof, and S. Burke, J. Chem. Phys. **105**, 9982 (1996).

[39]C. Adamo and V. Barone, J. Chem. Phys. **110**, 6158 (1999).

[40]J. Heyd, G. E. Scuseria, and M. Ernzerhof, J. Chem. Phys. **124**, 219906 (2006).

[41]A. Walsh, J. L. F. Da Silva, and S.-H. Wei, Phys. Rev. Lett. **100**, 256401 (2008).

[42]P. E. Blöchl, Phys. Rev. B **50**, 17953 (1994).

[43]G. Kresse and D. Joubert, Phys. Rev. B **59**, 1758 (1999).

[44]G. Kresse and J. Hafner, Phys. Rev. B **48**, 13115 (1993).

[45]G. Kresse and J. Furthmüller, Phys. Rev. B **54**, 11169 (1996).

[46]D. J. Wales and J. P. K. Doye, J. Phys. Chem. A **101**, 5111 (1997).

[47]B. V. Reddy, S. K. Nayak, S. N. Khanna, B. K. Rao, and P. Jena, Phys. Rev. B **59**, 5214 (1999).

[48]R. Hoppe, Angew. Chem. Internat. Edit. **9**, 25 (1970).

[49]R. Hoppe, Z. Kristallogr. **150**, 23 (1979).

[50]J. L. F. Da Silva, J. Appl. Phys. **109**, 023502 (2011).

[51]J. L. F. Da Silva, A. Walsh, and S.-H. Wei, Phys. Rev. B **80**, 214118 (2009).

[52]J. L. F. Da Silva, H. G. Kim, M. J. Piotrowski, M. J. Prieto, and G. Tremiliosi-Filho, Phys. Rev. B **82**, 205424 (2010).

[53]W. Zhang, L. Xiao, Y. Hirata, T. Pawluk, and L. Wang, Chem. Phys. Lett. **383**, 67 (2004).

[54]K. A. Gingerich and D. L. Cocke, J. Chem. Soc., Chem. Comm. **321**, 536 (1972).

[55]J. D. Langenberg and M. D. Morse, J. Chem. Phys. **108**, 2331 (1998).